

Peralkalinity in peraluminous granitic pegmatites. II. Evidence from experiments on carbonate formation in spodumene-bearing assemblages

YONGCHAO LIU^{1,2}, CHRISTIAN SCHMIDT^{2,*}, AND JIANKANG LI¹

¹MNR Key Laboratory of Metallogeny and Mineral Assessment, Institute of Mineral Resources, Chinese Academy of Geological Sciences, Beijing 100037, China

²GFZ German Research Centre for Geosciences, Telegrafenberg, 14473 Potsdam, Germany

ABSTRACT

Carbonate has often been identified in aqueous carbonic inclusions in spodumene-bearing and other pegmatites, but its origin remains unclear. Here, the conditions at which carbonate and hydrogen carbonate can be generated from spodumene, CO₂ and H₂O, were studied using a hydrothermal diamond-anvil cell (HDAC) and Raman spectroscopy. In all experiments, spodumene persisted in aqueous carbonic solution up to the maximum temperature (600 to 800 °C). Heating of hydrogen carbonate/oxalate solutions produced CO₂- and HCO₃⁻-rich peralkaline fluids, which resulted in strong corrosion of spodumene (and polythionite-trilithionite) and, in one run, formation of zabuyelite [Li₂(CO₃)] crystals at low temperatures. The experiments indicate that the reaction of spodumene with CO₂ and H₂O requires a peralkaline fluid to proceed rapidly. In addition, they show that spodumene crystallizes upon the heating of quartz, muscovite, and aqueous lithium carbonate solution. We conclude that if the aqueous fluid was rich in alkali hydrogen carbonate, zabuyelite in fluid inclusions in pegmatites can form both via a subsolidus reaction of CO₂-bearing fluid inclusion with the spodumene host or by trapping a peralkaline fluid early in the evolution of simple or complex pegmatites. The results of our experimental study strengthen the conclusion that, although counterintuitive, hydrogen carbonate-rich peralkaline fluids may be involved in the evolution of peraluminous granitic pegmatites, in which peralkaline minerals are normally absent or very rare.

Keywords: Zabuyelite, carbonate, hydrogen carbonate, CO₂, pegmatite, spodumene, hydrothermal diamond-anvil cell

INTRODUCTION

Fluid inclusions with nahcolite [NaH(CO₃)] and zabuyelite [Li₂(CO₃)] crystals in addition to aqueous carbonate/bicarbonate-rich solution and CO₂ have been reported to occur in graphic granite of simple pegmatites from the Klippeløkken granite quarry, east of Rønne, Bornholm Island, Denmark (Thomas et al. 2011) and in pegmatitic granites from the Marcação, Galo Branco, and Picuí quarries, in the Borborema Pegmatite Province, northeast-Brazil (Beurlen et al. 2014). Similarly, crystal-rich inclusions containing zabuyelite, CO₂, and quartz/cristobalite, as well as calcite, pollucite-analcime, albite, or cookeite, were found in spodumene from the Tanco, Jiajika, Muiâne, Bikita, Kamativi, Lacorne, Zhawulong, and other pegmatites (London 1986; Anderson et al. 2001; Lima et al. 2003; Thomas and Davidson 2010; Li and Chou 2016, 2017; Mulja and Williams-Jones 2018; Xiong et al. 2019). Macroscopic primary carbonates [calcite, calcioancylite-(Ce), rhodochrosite, siderite, and even zabuyelite] and carbonate-rich fluorapatite are generally rare in peraluminous granitic pegmatites, but there are several reports from well-studied localities, e.g., the Bennett, Berry-Havey, Dunton, Emmons, Mount Mica, and other pegmatites in Maine, U.S.A.; the Palermo No. 1 and

No. 2 Mines, New Hampshire, U.S.A.; the Foote Mine, North Carolina, U.S.A.; and the Tanco Mine, Manitoba, Canada (www.mindat.org).

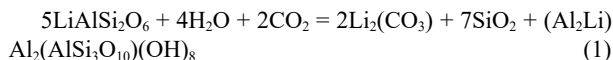
The origin of zabuyelite-bearing and generally of alkali carbonate- and hydrogen carbonate-bearing fluid inclusions in pegmatites is still debated. One opinion is that these carbonates formed by the reaction of carbon dioxide with a flux-rich peralkaline melt, which exsolved from a granitic melt (Thomas et al. 2006a, 2006b, 2011; Beurlen et al. 2014; Thomas and Davidson 2015, 2016). London (2015) pointed to experimental evidence that melt-melt immiscibility is not required to produce flux-rich hydrous granitic melts, stated again that “exceedingly hydrous, alkaline, flux-rich” melt can simply be generated in the boundary layers of crystals growing rapidly in undercooled melts, and interprets such inclusions as a product of heterogeneous trapping (i.e., after phase separation) because of their high compositional variability. In the case of the Jiajika spodumene pegmatite, carbonate and cookeite are thought to be of primary origin (Li and Chou 2017; Ding et al. 2020). Anderson et al. (2001) and Anderson (2013, 2019) argued that, at least in the Tanco pegmatite, zabuyelite, cristobalite, and cookeite in crystal-rich fluid inclusions in spodumene were formed by a late-stage subsolidus reaction of spodumene with entrapped or infiltrating CO₂-rich aqueous fluid. However, the reaction proposed by Anderson (2019):

* E-mail: Christian.Schmidt@gfz-potsdam.de

TABLE 1. Experimental conditions and run products identified using Raman spectroscopy

Run no.	Initial solid charge	$T_{\text{HLV-LI}}$ (°C)	T_{max} (°C)	Dwell time (days)
YLCS1	Qtz(1.5) + Ms(0.5) + $\text{Li}_2(\text{CO}_3)$ (excess)	130.3/279.4	700	/
YLCS2	Spd(5.9) + $\text{NaH}(\text{CO}_3)$ (9.9)	325.0/313.4	600	3 (100 °C)
YLCS3	Spd(3.9) + $\text{H}_2(\text{C}_2\text{O}_4) \cdot 2\text{H}_2\text{O}$ (10.8)	273.9/274.7	800	1 (100 °C)
YLCS4	Spd(3.9) + Qtz(8.1) + Ms(2.7) + San(3.2) + $\text{H}_2(\text{C}_2\text{O}_4) \cdot 2\text{H}_2\text{O}$ (12.1)	347.0/342.0	750	3 (200 °C)
YLCS5	Spd(4.4) + Qtz(2.7) + Ms(4.0) + San(3.0) + $\text{H}_2(\text{C}_2\text{O}_4) \cdot 2\text{H}_2\text{O}$ (12.1)	332.5/320.5	600	5 (200 °C)
YLCS6	Spd(1.1) + Qtz(3.5) + Ms(1.7) + San(1.9) + $\text{K}_2(\text{C}_2\text{O}_4) \cdot \text{H}_2\text{O}$ (13.0)	553.2/551.6	600	5 (200 °C)
YLCS7	Spd(1.2) + Qtz(3.8) + Ms(1.4) + San(2.9) + $\text{KH}(\text{CO}_3)$ (11.5)	421.5/322.4	600	3 (200 °C)
YLCS8	Spd(1.9) + Qtz(5.6) + "Lpd"(2.0) + Ab(2.5) + $\text{NaH}(\text{CO}_3)$ (17.2)	253.4/204.1	600	3 (200 °C), 3 (100 °C)
YLCS9	Spd(3.5) + Qtz(7.6) + "Lpd"(2.0) + Ab(4.0) + $\text{Na}_2(\text{C}_2\text{O}_4)$ (16.1)	509.0/476.4	600	4 (200 °C)

Notes: The numbers in parentheses in the initial solid charge column represent the approximate volume percentages of each loaded solid relative to the sample chamber volume based on measured sizes from microscopy. Qtz = quartz; Ms = muscovite; Spd = spodumene; Ab = albite; Anl = analcime; Nah = nahcolite; Zbl = zabuyelite; San = sanidine; Kfs = K-feldspar; "Lpd" = polyolithionite-trilithionite ("lepidolite"); Klc = kalicinite; Gl = glass. $T_{\text{HLV-LI}}$ = temperature of bubble disappearance measured during heating/after cooling. T_{max} = maximum temperature of each run. Dwell time = time the samples remained at 200 or 100 °C after cooling from T_{max} . b.d.l. = HCO_3^- and CO_3^{2-} below detection limit. (Table extends on next page)



requires a basic pH to proceed toward carbonate formation because of



but high pH values are uncommon in natural hydrothermal fluids because they can only be attained after consumption of $\text{H}_4\text{SiO}_4(\text{aq})$.

Here, we therefore carried out a series of experiments to constrain conditions at which carbonate can be generated from spodumene, CO_2 , and H_2O . To this end, we used a hydrothermal diamond-anvil cell and Raman spectroscopy to study the behavior of spodumene-bearing assemblages in aqueous carbonic fluids and to observe reactions in situ at high temperature. The starting mineral assemblages included only rock-forming lithium pegmatite minerals (quartz, albite, K-feldspar, muscovite, or polyolithionite-trilithionite, besides spodumene). An aqueous fluid with CO_2 at different pH was produced by decomposition of alkali oxalate or oxalic acid, or by addition of alkali hydrogen carbonate.

EXPERIMENTAL METHODS

The starting materials were natural spodumene (Spd) from the Pala Chief Mine and polyolithionite-trilithionite ("lepidolite") ("Lpd") from the Elizabeth R. Mine, both in Pala pegmatite district, San Diego County, California, U.S.A., albite (Ab) from the Rutherford No. 2 pegmatite, Amelia County, Virginia, U.S.A., natural quartz (Qtz) and muscovite (Ms) from unknown locations (pegmatites) in Brazil, and sanidine (San) from Itrongay, Anosy, Madagascar. All samples were optically clear and did not contain microscopically visible solid or fluid inclusions. Chemical reagents used in the experiments included $\text{Li}_2(\text{CO}_3)$ (99.99%, Merck), $\text{NaH}(\text{CO}_3)$ (ACS for analysis, Merck), $\text{KH}(\text{CO}_3)$ (99.7–100.5%, Alfa Aesar), $\text{H}_2(\text{C}_2\text{O}_4) \cdot 2\text{H}_2\text{O}$ (GR for analysis, Merck), $\text{Na}_2(\text{C}_2\text{O}_4)$ (99.9%, VWR), and $\text{K}_2(\text{C}_2\text{O}_4) \cdot \text{H}_2\text{O}$ (99.5–101.0%, Merck).

The experiments were performed using a modified Bassett-type hydrothermal diamond-anvil cell (Bassett et al. 1993; Schmidt and Chou 2012). The sample chamber was a cylindrical hole with an initial diameter of 400 μm and an initial height of 125 μm in an iridium gasket between the diamond culets. A rhenium gasket was used in run YLCS1. The sample chamber was heated via two independent nickel-chromium coils using TDK Lambda Z60 power supplies and Eurotherm 2408 temperature controllers, which held the target temperature within ± 0.3 °C. The temperature in the sample chamber was monitored using two K-type (Ni-Cr/Ni) thermocouples in contact with the upper and lower diamonds, and it was calibrated by repeated measurements of the α - β transition temperature of quartz (574 °C, 0.1 MPa). A Leica microscope equipped with a Nikon 20 \times objective (numerical aperture 0.25) and a digital camera was used to observe the sample chamber, and to acquire images of the whole sample chamber in real time.

The sizes of all crystals to be loaded were measured under the microscope, with an error of about ± 1 μm perpendicular to the optical axis of the lens and

approximately ± 5 μm parallel to it. Then, the sample chamber was loaded with these crystals and distilled water, and an air bubble was allowed to grow before the chamber was sealed. At the start of each run, the charges were heated, and the temperature was held at target temperatures ranging from 600 to 800 °C for up to 2 h. Subsequently, the samples were cooled to 200 or 100 °C and remained at these temperatures for 1–5 days. During the experiments, the HDAC was flushed with an Ar+1% CH_4 gas mixture to protect the cell from oxidation.

At the end of each run, the solid phases, solution, and bubble in the closed sample chamber were analyzed using a HORIBA Jobin Yvon LabRAM HR800 Vis Raman spectrometer equipped with a Synapse 2048 \times 512 back-illuminated CCD-detector, a Laser Quantum Torus 532 DPSS laser for excitation at 532.17 nm, a grating of 1800 lines/mm, a confocal pinhole diameter of 100 μm , and an Olympus 20 \times SLMP objective (numerical aperture 0.25). Spectra of the solid phases at 200–1200 cm^{-1} and spectra of the bubble centered at 1070, 1600, 2200, 2900, and 4156 cm^{-1} were recorded with 4 accumulations of 20 s each. Spectra of the solution centered at 1070 cm^{-1} were recorded with 16 accumulations of 20 s each.

RESULTS

The experimental conditions and results of nine runs are summarized in Table 1.

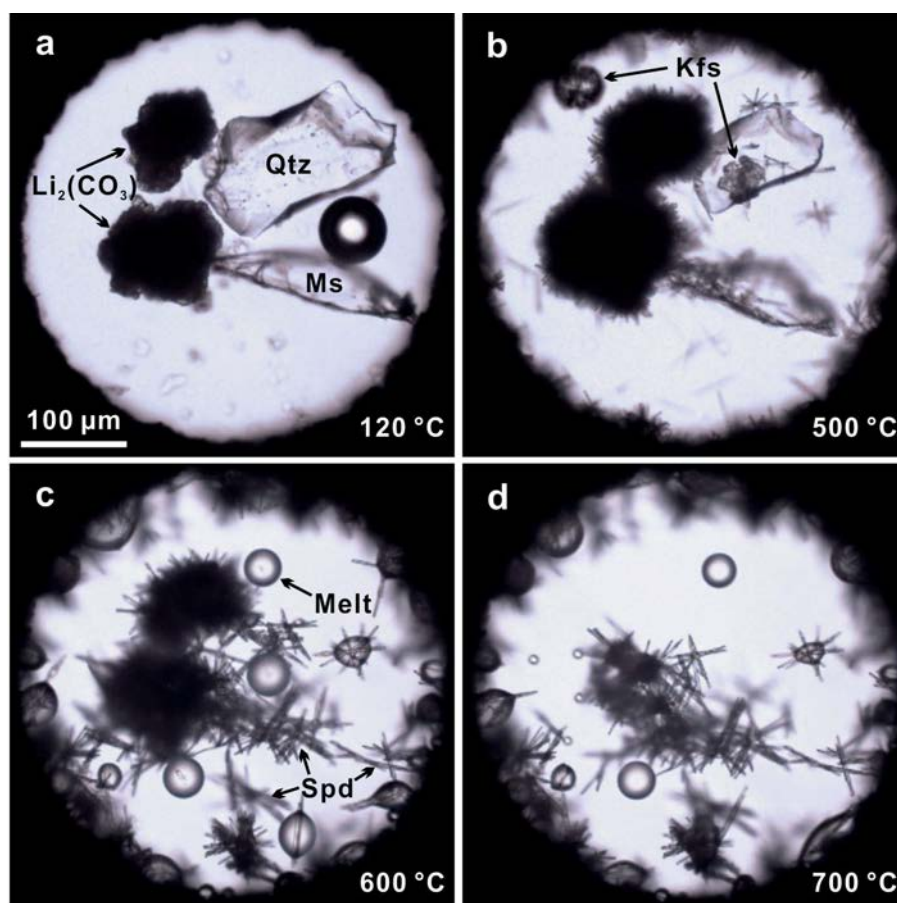
In run YLCS1 [$\text{Qtz} + \text{Ms} + \text{Li}_2(\text{CO}_3) + \text{H}_2\text{O}$], the only run in which a Re gasket was used, the sample chamber contained quartz, muscovite, $\text{Li}_2(\text{CO}_3)$ crystalline powder, an aqueous solution, and a bubble at the start of the experiment (Fig. 1a). At 500 °C, quartz and muscovite had become much smaller, and numerous acicular crystals had nucleated and grown (Fig. 1b). After holding the temperature at 500 °C for 2 h, the run was cooled to room temperature, and Raman spectra showed that K-feldspar had formed and that zabuyelite was still present. Then, the sample was heated to 600 °C for 2 h, at which temperature quartz and muscovite had completely dissolved, and melt droplets and numerous acicular spodumene crystals had appeared (Fig. 1c). Solid lithium carbonate completely dissolved during further heating to 700 °C (Fig. 1d). Raman spectra at room temperature at the end of the experiment showed that the acicular crystals were spodumene (Raman bands at about 245, 292, 333, 351, 388, 437, 519, 580, 703, and 1068 cm^{-1} ; Fig. 2; Lafuente et al. 2015), that glass was present, that the aqueous solution contained HCO_3^- (Raman bands at about 640, 670, and 1019 cm^{-1}) but no detectable CO_3^{2-} (Figs. 2 and 3), and that the vapor bubble contained CO_2 and CH_4 (Fig. 4). Three intense bands in the spectra of the solution, at about 330, 920, and 971 cm^{-1} (Fig. 2), are assigned to the perrenate ion, ReO_4^- (Woodward and Roberts 1956; Eysel and Kanellakopoulos 1993). We used Ir gaskets in the other subsequent runs to ensure inert behavior and avoid intense Raman bands in a region of interest.

In run YLCS2 [$\text{Spd} + \text{NaH}(\text{CO}_3) + \text{H}_2\text{O}$], the vapor-saturated dissolution temperature of nahcolite was 150.6 °C, which cor-

TABLE 1—EXTENDED

Run no.	Solids	Aqueous solution	Vapor bubble	Additional observations during heating
YLCS1	Spd, Gl	HCO ₃ ⁻	CO ₂ , CH ₄	Complete consumption of Li ₂ (CO ₃), Qtz, and Ms
YLCS2	Spd, Ab, Anl, Nah, Zbl	HCO ₃ ⁻ , CO ₃ ²⁻	CO ₂ , CH ₄	Strong corrosion of Spd
YLCS3	Spd, Gl	b.d.l.	CO ₂ , CO, CH ₄	Partial dissolution of Spd
YLCS4	Spd, Qtz, Ms, Kfs	b.d.l.	CO ₂ , CO, CH ₄ , H ₂	Very little, if any, changes of Spd, Qtz, Ms, Kfs
YLCS5	Spd, Qtz, Ms, Kfs	b.d.l.	CO ₂ , CO, CH ₄ , C ₂ H ₆ , H ₂	Very little, if any, changes of Spd, Qtz, Ms, Kfs
YLCS6	Spd, Kfs, Gl	HCO ₃ ⁻ , CO ₃ ²⁻	CO ₂ , CH ₄ , H ₂	Complete melting of Qtz and Ms; Klc formed when cell was opened
YLCS7	Spd, Qtz, Ms, Kfs	HCO ₃ ⁻ , CO ₃ ²⁻	CO ₂ , CH ₄	Corrosion of Qtz, nucleation of crystals on Spd and Ms
YLCS8	Spd, Qtz, "Lpd", Ab, Gl	HCO ₃ ⁻	CO ₂ , CH ₄	Growth of Ab, corrosion of Spd, "Lpd", Qtz
YLCS9	Spd, Qtz, Ab, Nah	HCO ₃ ⁻ , CO ₃ ²⁻	CH ₄ , C ₂ H ₆ , C ₃ H ₈ , H ₂	"Lpd" replaced by Ab, corrosion of Qtz

FIGURE 1. Photographs of the sample chamber in run YLCS1. Qtz = quartz; Ms = muscovite; Kfs = K-feldspar; Zbl = zabuyelite; Spd = spodumene. (a) The sample chamber at 120 °C still containing the initial phases quartz, muscovite, lithium carbonate, aqueous solution, and a bubble, which disappeared at 130.3 °C during further heating. (b) Run YLCS1 at 500 °C, (c) 600 °C, and (d) 700 °C. (Color online.)



responds to 26.8 mass% NaH(CO₃) relative to water (Linke and Seidell 1965). Further heating of the hydrogen carbonate solution produced significant CO₂ (Schmidt 2014). Numerous acicular crystals appeared at 509 °C. At 580 °C, analcime and albite nucleated and grew simultaneously with the dissolution of the acicular crystals (Fig. 5a) until the latter was completely consumed after the temperature was set to 600 °C (Fig. 5b). The initially loaded two spodumene crystals had become much smaller at 600 °C. After cooling to 22 °C, the solid phases in the sample chamber were identified using Raman spectroscopy and included nahcolite, spodumene, albite, and analcime with well-developed crystal faces (Figs. 5c and 6). The sample was heated again to 100 °C and remained at this temperature for 3 days, during which time prismatic zabuyelite crystals formed (Fig. 5d). Zabuyelite was identified using Raman spectroscopy (its most

intense peak is at 1091 cm⁻¹; Fig. 6; Lafuente et al. 2015). This had to be done within about a minute after the start of cooling, when the sample was still hot because the solubility of zabuyelite increases with decreasing temperature (Smith et al. 1971) and thus the zabuyelite crystals dissolved upon cooling. Raman spectroscopy at room temperature showed HCO₃⁻ and CO₃²⁻ in the solution (Fig. 3) and CO₂ and CH₄ in the vapor bubble (Fig. 4).

In run YLCS3 [Spd+H₂(C₂O₄)+H₂O], the sample after loading consisted of spodumene, oxalic acid solution, and a bubble. The solute concentration was 1.867% (mol/mol) H₂(C₂O₄) relative to water (Omar and Ulrich 2006) based on the final melting temperature of 19.0 °C of the oxalate crystals generated during freezing with liquid nitrogen. The loaded spodumene crystal showed no obvious changes after heating to 600 °C (Fig. 7a). During further heating to 800 °C, the edges of the spodumene

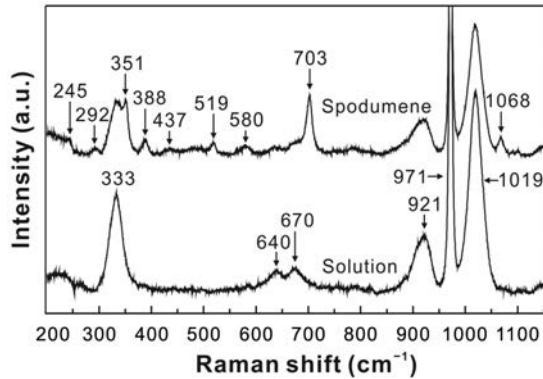


FIGURE 2. Raman spectra of aqueous solution and a mixture of spodumene and solution obtained at room temperature at the end of run YLCS1.

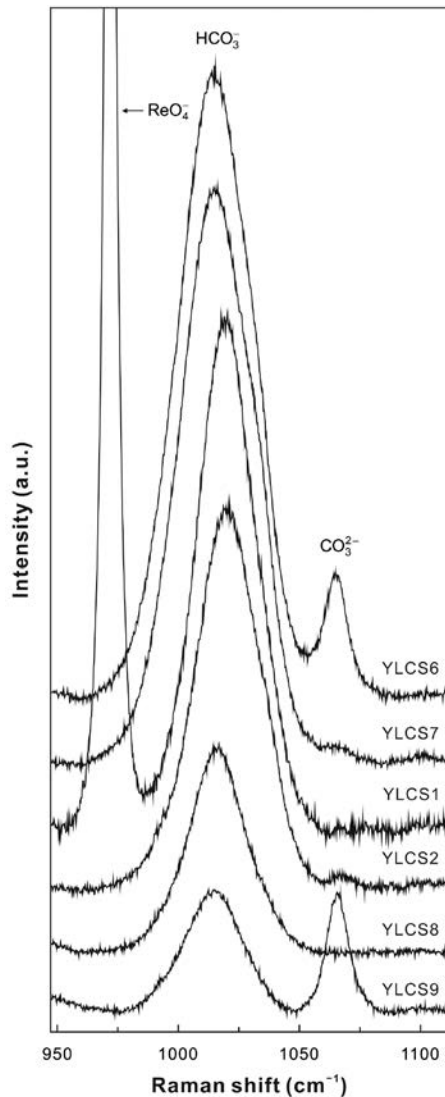


FIGURE 3. Raman spectra of the aqueous solution obtained at room temperature and vapor pressure at the end of each run in Table 1.

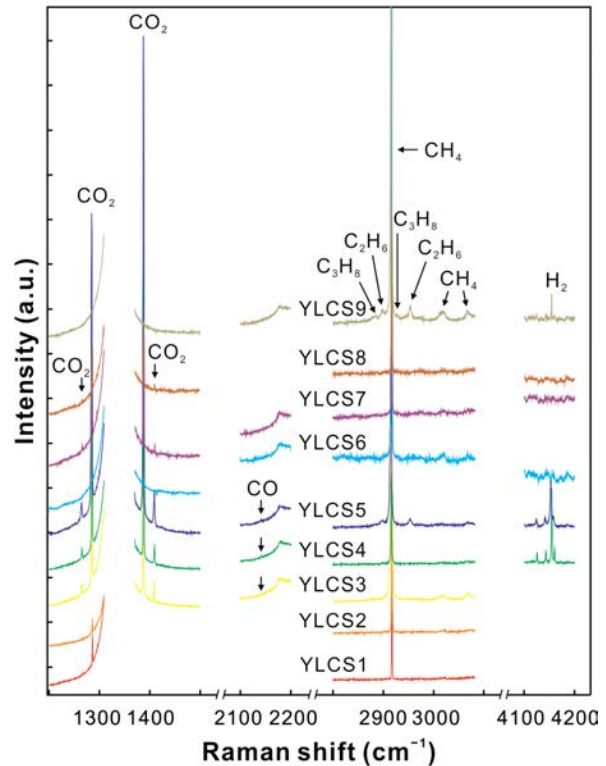


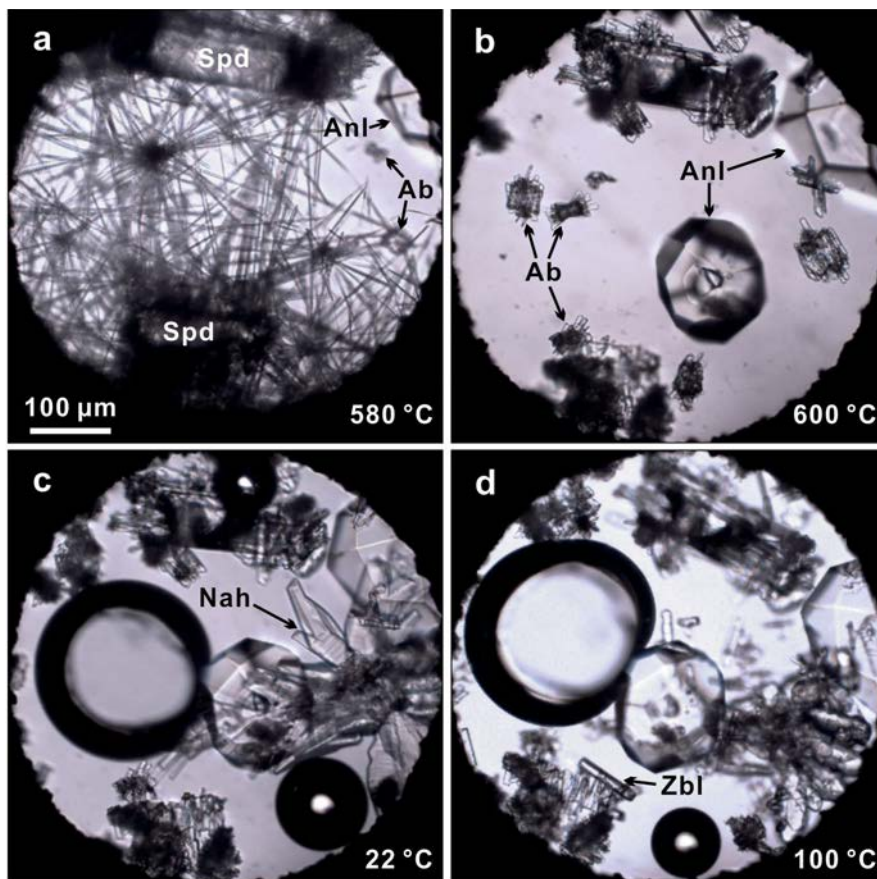
FIGURE 4. Raman spectra of the vapor bubble obtained at room temperature at the end of each run in Table 1.

crystal became round and melt globules formed. Subsequent cooling caused exsolution of additional melt droplets from the solution. At the end of the run, the sample chamber contained spodumene, glass beads, aqueous solution, and vapor. No further changes were observed during subsequent dwell at 100 °C for 1 day (Fig. 7b). Raman analysis showed CO_2 , CH_4 , and CO in the bubble (Fig. 4), but did not detect HCO_3^- and CO_3^{2-} in the solution.

In runs YLCS4 and YLCS5 [$\text{Spd}+\text{Qtz}+\text{Ms}+\text{San}+\text{H}_2(\text{C}_2\text{O}_4)+\text{H}_2\text{O}$], the vapor-saturated dissolution temperatures of the oxalic acid crystals were 75.0 and 68.0 °C, which correspond to 14.66% (mol/mol) and 11.33% (mol/mol) $\text{H}_2(\text{C}_2\text{O}_4)$, respectively (Omar and Ulrich 2006). No obvious reaction of spodumene was observed when the temperature was raised to 750 °C (YLCS4) and 600 °C (YLCS5). After heating, the samples were cooled to 200 °C and remained at this temperature for 3 and 5 days, respectively (Table 1), without noticeable changes of their microscopic images. Raman analysis of the quenched samples showed that the vapor in both runs contained CO_2 , CH_4 , H_2 , and CO , and additionally C_2H_6 in run YLCS5 (Fig. 4). Furthermore, HCO_3^- and CO_3^{2-} were not detected in the solutions.

The initial assemblage of run YLCS6 consisted of $\text{Spd}+\text{Qtz}+\text{Ms}+\text{San}+\text{K}_2(\text{C}_2\text{O}_4)\cdot\text{H}_2\text{O}+\text{liquid H}_2\text{O}+\text{vapor}$. The vapor-saturated dissolution temperature of the potassium oxalate crystals was 57.1 °C, which corresponds to 1.027 molal $\text{K}_2(\text{C}_2\text{O}_4)$ (Menczel et al. 2004). During heating, many CO_2 -rich bubbles were generated due to oxalate decomposition (Fig. 8a). The loaded quartz and muscovite crystals diminished their size rapidly until their complete disappearance by melting at 500 °C (Fig. 8b). During

FIGURE 5. Photographs of the sample chamber in run YLCS2 at 580 °C (a), 600 °C (b), after cooling to 22 °C (c), and at 100 °C after second heating (d). Ab = albite; Anl = analcime; Spd = spodumene; Nah = nahcolite; Zbl = zabuyelite. (Color online.)



further heating to 600 °C, the CO₂-rich bubbles disappeared, and a portion of the melt dissolved (Fig. 8c). Subsequently, the sample was held at 200 °C for 5 days, without optically noticeable reaction during that time. Raman spectroscopy at ambient temperature showed that solid phases were spodumene remnant, glass, and many small K-feldspar crystals, particularly on the surface of the glass, and that the aqueous solution contained HCO₃⁻ and CO₃²⁻ (Fig. 3) and the vapor bubble CH₄, CO₂, and H₂ (Fig. 4). After the cell was opened, water evaporated, and kalicinite [KH(CO₃)] crystals formed on the sample chamber wall (Fig. 8d). Kalicinite was identified based on the Raman spectrum (peaks at 183, 636, 676, 832, and 1029 cm⁻¹, Lafuente et al. 2015).

In the case of the Spd+Qtz+Ms+San+KH(CO₃)+H₂O run (YLCS7), we measured a vapor-saturated dissolution temperature of KH(CO₃) of 60.8 °C, which corresponds to a solute concentration of 39.8 mass% (Linke and Seidell 1965). Upon heating, many bubbles nucleated around 345 °C (Fig. 9a). When the temperature was raised to 424 °C, numerous small crystals formed on the surfaces of spodumene and muscovite (Fig. 9b). At 600 °C, the quartz crystal had become much smaller, and many crystals had nucleated on spodumene and muscovite (Fig. 9c). No changes were observed optically during the subsequent dwell at 200 °C for three days. At the end of the run, the solid phases at room temperature included spodumene and muscovite remnants, quartz with crystal faces that had formed during rapid growth

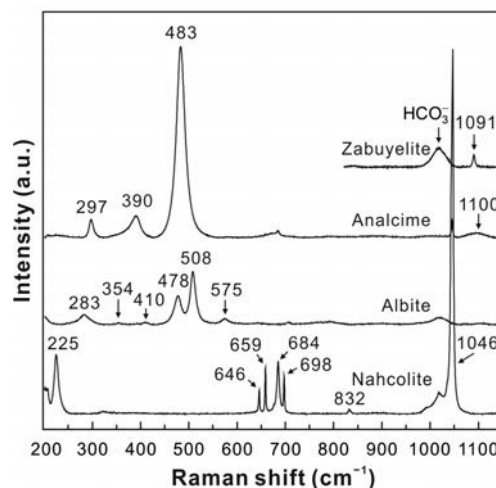
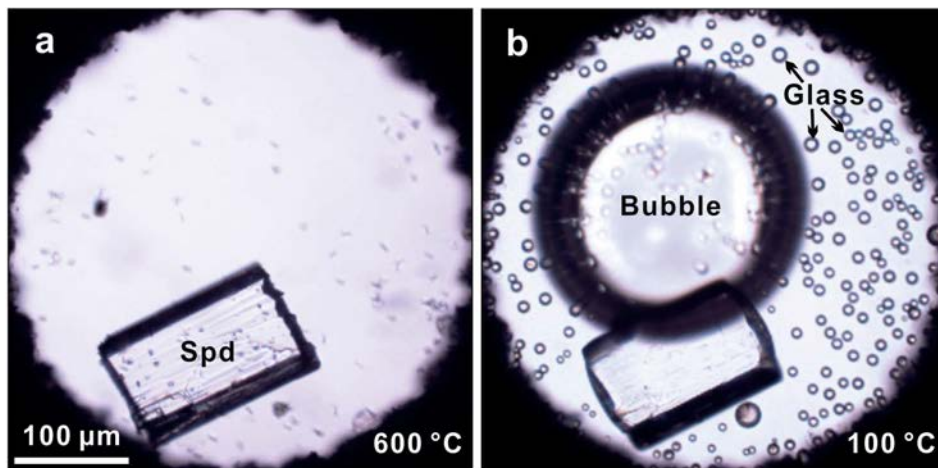


FIGURE 6. Raman spectra of the solid phases obtained at room temperature (spectrum of zabuyelite obtained at temperature below 100 °C) and vapor pressure at the end of run YLCS2.

upon cooling, initial K-feldspar, and many small K-feldspar crystals on spodumene and muscovite (Fig. 9d). Raman spectroscopy indicated HCO₃⁻ and CO₃²⁻ in the solution (Fig. 3) and CO₂ and CH₄ in the vapor (Fig. 4).

Run YLCS8 [Spd+Qtz+“Lpd”+Ab+NaH(CO₃)+H₂O] had

FIGURE 7. Photographs of the sample chamber in run YLCS3 at 600 °C (a) and 100 °C after cooling from 800 °C (b). Spd = spodumene. (Color online.)



a $\text{NaH}(\text{CO}_3)$ concentration of 14.3 mass% at the start of the experiment, as determined from the vapor-saturated dissolution temperature of nahcolite of 65.3 °C (Linke and Seidell 1965). Upon heating, quartz became rapidly smaller and crystals formed on the surface of polyolithionite-trilithionite as the temperature approached 560 °C (Fig. 10a). Further heating to 600 °C caused strong corrosion of spodumene, growth of the loaded albite crystal with development of crystal faces, and growth of numer-

ous small crystals on spodumene and polyolithionite-trilithionite (Fig. 10b). Then, the sample was cooled and remained at 200 °C for 3 days, followed by 3 days at 100 °C, without optically noticeable changes. At the end of the run, the solid phases as identified by Raman spectroscopy included a large albite crystal, many small albite crystals, glass, and the remnants of spodumene, quartz, and polyolithionite-trilithionite. Moreover, the aqueous solution contained HCO_3^- but $\text{CO}_3^{2-}(\text{aq})$ was below the lower

FIGURE 8. Photographs of the sample chamber in run YLCS6 at 363 °C (a), 500 °C (b), and 600 °C (c). Spd = spodumene, Qtz = quartz, Kfs = K-feldspar, Ms = muscovite. (d) Kalicinite $[\text{KH}(\text{CO}_3)]$ crystals (Klc) formed on the sample chamber wall when the cell was opened later. (Color online.)

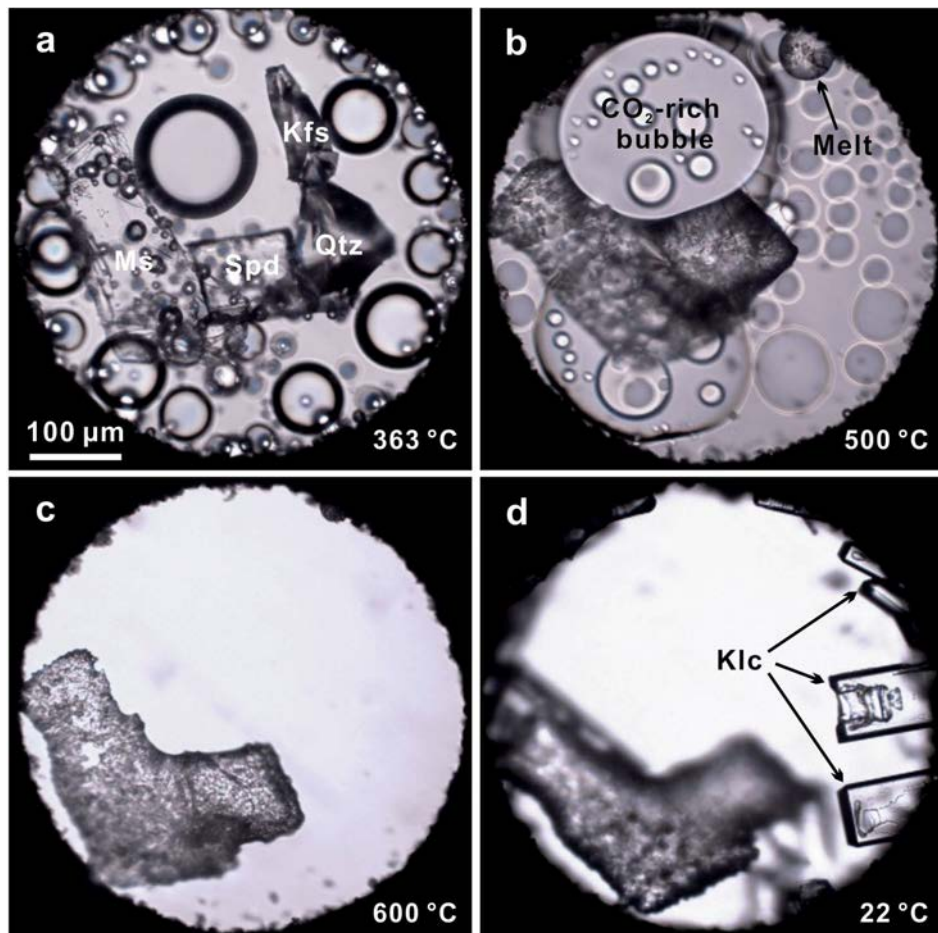
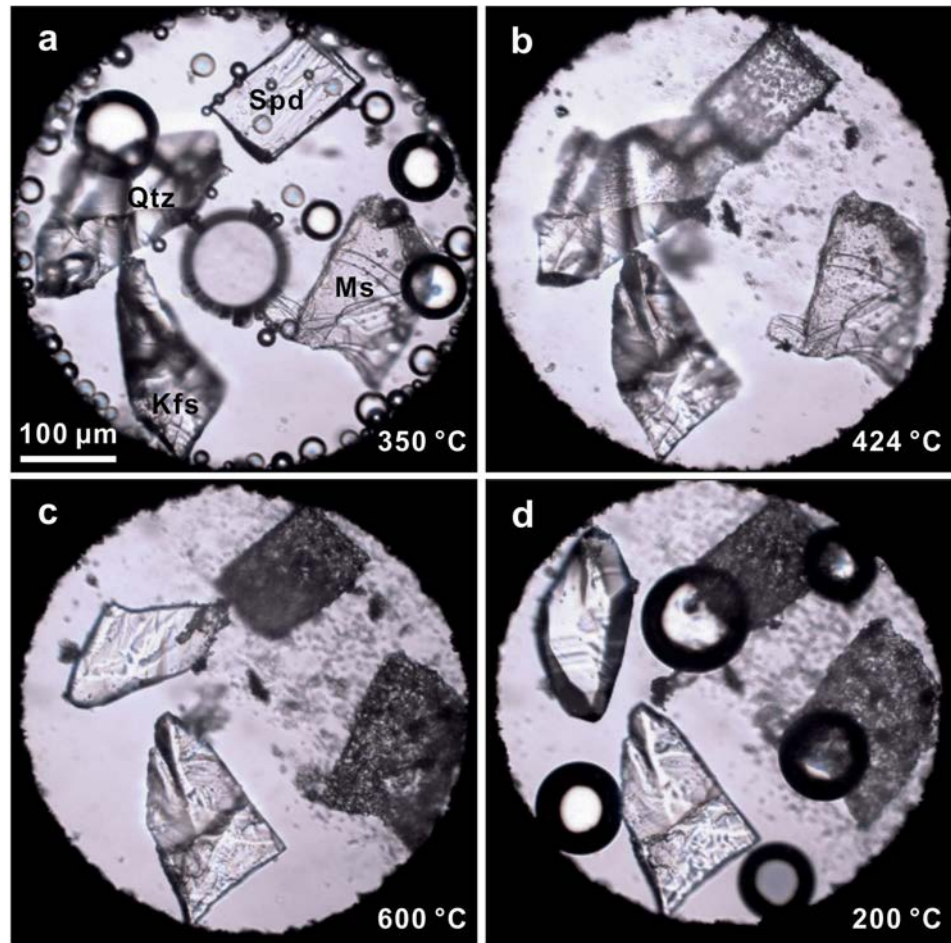


FIGURE 9. Photographs of the sample chamber in run YLCS7 at 350 °C (a), 424 °C (b), 600 °C (c), and 200 °C after cooling from 600 °C (d). Spd = spodumene; Qtz = quartz; Ms = muscovite; Kfs = K-feldspar. (Color online.)



detection limit (Fig. 3), and the CO_2 and CH_4 were observed in the vapor phase (Fig. 4).

We did not obtain the salt concentration of the last experiment YLCS9 [Spd+Qtz+“Lpd”+Ab+Na₂(C₂O₄)+H₂O] because no solubility data were available for Na₂(C₂O₄) vapor-saturated dissolution temperatures near the measured temperature of 379.0 °C. The sodium oxalate concentration in this run was much higher than the maximum concentration of the solubility data reported in the literature (0.367 molal at 60 °C; Menczel et al. 2004). Many bubbles appeared and polyolithionite-trilithionite started to change its optical appearance near the dissolution temperature of the sodium oxalate crystal (Fig. 11a). At the highest temperature of the run of 600 °C, quartz was strongly corroded, and numerous small crystals formed on the surfaces of polyolithionite-trilithionite and spodumene. Upon cooling, the quartz crystal grew and developed faces (Fig. 11b). No further changes were observed during the following dwell of four days at 200 °C. Then, the sample was cooled to room temperature, which caused the formation of acicular crystals. Raman spectroscopic inspection at the end of the experiment showed that the acicular crystals were nahcolite, that spodumene and quartz were present, and that polyolithionite-trilithionite was completely replaced by small albite crystals. Moreover, HCO_3^- and CO_3^{2-} were found in the solution (Fig. 3), and CH_4 , C_2H_6 , C_3H_8 , and H_2 in the vapor bubble (Fig. 4).

DISCUSSION

The objective of our experimental study was the identification of conditions of carbonate formation in spodumene-bearing pegmatites. Run YLCS1 showed that spodumene could crystallize if the pegmatite-forming minerals quartz and muscovite react with aqueous lithium carbonate fluids. Experiments YLCS2 to YLCS9 explored reactions of spodumene-bearing mineral assemblages with aqueous Na- or K-hydrogen carbonate or with Na- or K-oxalate solutions or oxalic acid. Carbon dioxide was generated in all experiments by heating of carbonate, hydrogen carbonate, or oxalate solutions, except in YLCS9, which was at more reduced conditions suggested by the strong Raman band intensity of CH_4 and the detection of H_2 , C_2H_6 , and C_3H_8 (Fig. 4), perhaps due to a carbohydrate contamination during loading. Carbonate dissolved in the aqueous fluid was observed at the end of four of these runs, i.e., YLCS2 [NaH(CO₃) starting solution], YLCS7 [KH(CO₃) starting solution], YLCS9 [Na₂(C₂O₄) starting solution], and YLCS6 [K₂(C₂O₄) starting solution]. Run YLCS2 was the only experiment in which carbonate precipitated (zabuyelite during dwell at 100 °C). Hydrogen carbonate (nahcolite or kalicinite) precipitated at the end of experiments YLCS9 and YLCS6 that had no HCO_3^- in the starting solutions. Notably, the fluid in all of these runs was peralkaline. None of the three runs in which oxalic acid was used as the source of CO_2 showed detectable carbonate or hydrogen carbonate in the solution even after 5 days of dwell at

FIGURE 10. Photographs of the sample chamber in run YLCS8 at 570 °C (a) and 600 °C (b). Spd = spodumene; Qtz = quartz; “Lpd” = polyolithionite-trilithionite (“lepidolite”); Ab = albite. (Color online.)

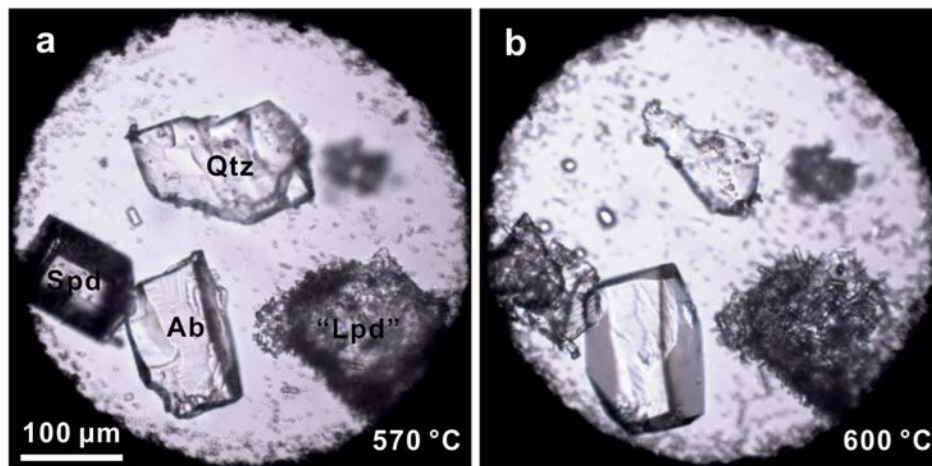
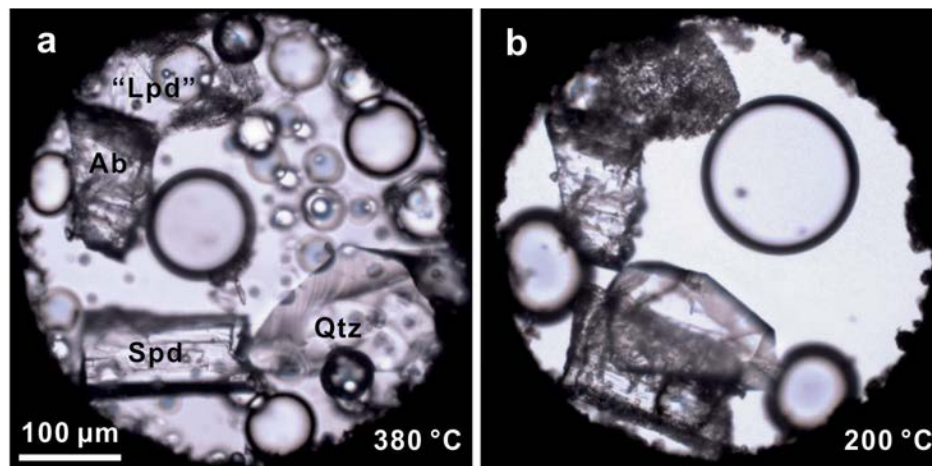


FIGURE 11. Photographs of the sample chamber in run YLCS9 at 380 °C (a) and 200 °C (b) after cooling from 600 °C. Spd = spodumene; Qtz = quartz; “Lpd” = polyolithionite-trilithionite (“lepidolite”); Ab = albite. (Color online.)



200 °C, or strong corrosion of spodumene. Therefore, zabuyelite is unlikely to form by reaction of spodumene with CO₂ and H₂O in the inclusions as proposed by Anderson (2019), unless the fluid had high alkalinity. This conclusion is somewhat counterintuitive for peraluminous granitic pegmatites because peraluminous minerals crystallize in all stages of their evolution, from early biotite, schorl and almandine in border zones to late and very late phyllosilicates (e.g., cookeite, or montmorillonite and kaolinite as pocket clays), and one would expect minerals typical for alkaline pegmatites if peralkaline fluids were present. Indeed, such minerals have been reported from peraluminous granitic pegmatites, e.g., nepheline in fluid inclusions or rimming K-feldspar (Rickers et al. 2006; Thomas et al. 2006b). The small scale of their occurrence suggests the total amount of peralkaline fluids generated during crystallization of peraluminous granitic pegmatites was relatively small but may be underestimated due to the high reactivity destroying most evidence of preexisting peralkalinity (Thomas et al. 2006b).

IMPLICATIONS

The results of our experiments indicate that an alkaline fluid was crucial in the formation of the crystal-rich inclusions in spodumene and rule out infiltration or trapping of a non-alkaline H₂O-CO₂ fluid. They support what Černý (1972) inferred

already about 50 years ago, i.e., that secondary minerals such as cesian analcime, cesian beryl, cookeite, adularia, albite, lithiophosphate, apatite, montmorillonite-illite, calcite, and quartz in the spodumene-rich zones of the Tanco pegmatite were products of residual alkaline solutions reacting with primary phases. A similar paragenesis was observed in our study in run YLCS2 through heating to 600 °C (Fig. 5). However, our experimental results do not clarify if such an alkaline fluid was generated via melt-melt immiscibility or by boundary layer formation (e.g., Thomas et al. 2006a; London 2009). The latter is in accord with experimental evidence for peraluminous granitic compositions (London 2015) and accounts for the fact that peraluminous phases (mostly biotite, almandine, tourmaline-group minerals, muscovite, polyolithionite-trilithionite, and clay minerals in “pockets”) crystallize from very early until very late stages of the evolution of such pegmatites, and are much more abundant than peralkaline minerals. Therefore, the bulk of the pegmatite-forming liquid must remain peraluminous, and alkaline melts and fluids can only develop in a relatively small volume during crystallization.

ACKNOWLEDGMENTS

We thank Pietro Vignola, Rainer Thomas, and an anonymous reviewer for their helpful comments to improve an earlier version of the manuscript. Collection of spodumene from the Pala Chief Mine and of polyolithionite-trilithionite from the

Elizabeth R. Mine was permitted by the owner, Jeff Swanger. Yongchao Liu is grateful to Monika Koch-Müller for providing the opportunity to study at Section 3.6 Chemistry and Physics of Earth Materials, GFZ Potsdam.

FUNDING

Jiankang Li and Yongchao Liu acknowledge support from the National Key R&D program of China (2019YFC0605200), the National Natural Science Foundation of China (41872096), and the Chinese National Non-profit Institute Research Grant of CAGS-IMR (JYYWF201814). Yongchao Liu acknowledges support from the China Scholarship Council (201908110333).

REFERENCES CITED

- Anderson, A.J. (2013) Are silicate-rich inclusions in spodumene crystallized aliquots of boundary layer melt? *Geofluids*, 13, 460–466.
- (2019) Microthermometric behavior of crystal-rich inclusions in spodumene under confining pressure. *Canadian Mineralogist*, 57, 853–865.
- Anderson, A.J., Clark, A.H., and Gray, S. (2001) The occurrence and origin of zabuyelite (Li_2CO_3) in spodumene-hosted fluid inclusions: Implications for the internal evolution of rare-element granitic pegmatites. *Canadian Mineralogist*, 39, 1513–1527.
- Bassett, W.A., Shen, A.H., Bucknum, M., and Chou, I.-M. (1993) A new diamond anvil cell for hydrothermal studies to 2.5 GPa and from -190 to 1200 °C. *Review of Scientific Instruments*, 64, 2340–2345.
- Beurlen, H., Thomas, R., Rodrigues da Silva, M.R., Müller, A., Rhede, D., and Soares, D.R. (2014) Perspectives for Li- and Ta-mineralization in the Borborema Pegmatite Province, NE-Brazil: A review. *Journal of South American Earth Sciences*, 56, 110–127.
- Černý, P. (1972) The Tanco pegmatite at Bernic Lake, Manitoba; VIII, Secondary minerals from the spodumene-rich zones. *Canadian Mineralogist*, 11, 714–726.
- Ding, X., Li, J.K., Chou, I.-M., Chen, Z.Y., and Li, S.H. (2020) Raman spectroscopic identification of cookeite in the crystal-rich inclusions in spodumene from the Jiajika lithium pegmatite deposit, China, and its geological implications. *European Journal of Mineralogy*, 32, 67–75.
- Eysel, H.H., and Kanellakopoulos, B. (1993) Raman spectra, absolute Raman intensities and electro-optical parameters of perchlorate, perchlorate and periodate ions in aqueous solution. *Journal of Raman Spectroscopy*, 24, 119–122.
- Lafuente, B., Downs, R.T., Yang, H., and Stone, N. (2015) The power of databases: the RRUFF project. In T. Armbruster and R.M. Danisi, Eds., *Highlights in Mineralogical Crystallography*, p. 1–30. De Gruyter.
- Li, J.K., and Chou, I.-M. (2016) An occurrence of metastable cristobalite in spodumene-hosted crystal-rich inclusions from Jiajika pegmatite deposit, China. *Journal of Geochemical Exploration*, 171, 29–36.
- (2017) Homogenization experiments of crystal-rich inclusions in spodumene from Jiajika lithium deposit, China, under elevated external pressures in a hydrothermal diamond-anvil cell. *Geofluids*, 2017, 1–12.
- Lima, A.M.C., Martins, T.C., Vieira, R.C., and Noronha, F. (2003) The study of fluid inclusions in petalite-bearing pegmatite-aplite veins of the Barroso-Álvao field (Northern Portugal). *Acta Mineralogica-Petrographica, Abstract Series*, 2, 111–112.
- Linke, W.F., and Seidell, A. (1965) *Solubilities of inorganic and metal-organic compounds*, vol. II, 4th ed. American Chemical Society, Washington, D.C.
- London, D. (1986) Magmatic-hydrothermal transition in the Tanco rare-element pegmatite: Evidence from fluid inclusions and phase-equilibrium experiments. *American Mineralogist*, 71, 376–395.
- (2009) The origin of primary textures in granitic pegmatites. *Canadian Mineralogist*, 47, 697–724.
- (2015) Reply to Thomas and Davidson on “A petrologic assessment of internal zonation in granitic pegmatites” (London, 2014a). *Lithos*, 212–215, 469–484.
- Menczel, B., Apelblat, A., and Korin, E. (2004) The molar enthalpies of solution and solubilities of ammonium, sodium and potassium oxalates in water. *The Journal of Chemical Thermodynamics*, 36, 41–44.
- Mulja, T., and Williams-Jones, A.E. (2018) The physical and chemical evolution of fluids in rare-element granitic pegmatites associated with the Lacome pluton, Québec, Canada. *Chemical Geology*, 493, 281–297.
- Omar, W., and Ulrich, J. (2006) Solid liquid equilibrium, metastable zone, and nucleation parameters of the oxalic acid–water system. *Crystal Growth & Design*, 6, 1927–1930.
- Rickers, K., Thomas, R., and Heinrich, W. (2006) The behavior of trace elements during the chemical evolution of the H_2O -, B-, and F-rich granite–pegmatite–hydrothermal system at Ehrenfriedersdorf, Germany: a SXRF study of melt and fluid inclusions. *Mineralium Deposita*, 41, 229–245.
- Schmidt, C. (2014) Raman spectroscopic determination of carbon speciation and quartz solubility in $\text{H}_2\text{O} + \text{Na}_2\text{CO}_3$ and $\text{H}_2\text{O} + \text{NaHCO}_3$ fluids to 600°C and 1.53 GPa. *Geochimica et Cosmochimica Acta*, 145, 281–296.
- Schmidt, C., and Chou, I.-M. (2012) The hydrothermal diamond anvil cell (HDAC) for Raman spectroscopic studies of geological fluids at high pressures and temperatures. In J. Dubessy, M.C. Caumon, and F. Rull, Eds., *Raman Spectroscopy Applied to Earth Science and Cultural Heritage*, 12, p. 247–276. EMU Notes in Mineralogy, Aberystwyth, U.K.
- Smith, S.H. Jr., Williams, D.D., and Miller, R.R. (1971) Solubility of lithium carbonate at elevated temperatures. *Journal of Chemical & Engineering Data*, 16, 74–75.
- Thomas, R., and Davidson, P. (2010) Hambergite-rich melt inclusions in morganite crystals from the Muiane pegmatite, Mozambique and some remarks on the paragenesis of hambergite. *Mineralogy and Petrology*, 100, 227–239.
- (2015) Comment on “A petrologic assessment of internal zonation in granitic pegmatites” by David London (2014). *Lithos*, 212–215, 462–468.
- (2016) Revisiting complete miscibility between silicate melts and hydrous fluids, and the extreme enrichment of some elements in the supercritical state—Consequences for the formation of pegmatites and ore deposits. *Ore Geology Reviews*, 72, 1088–1101.
- Thomas, R., Webster, J.D., and Davidson, P. (2006a) Understanding pegmatite formation: The melt and fluid inclusion approach. *Mineralogical Association Canada Short Course*, 36, 189–210.
- Thomas, R., Webster, J.D., Rhede, D., Seifert, W., Rickers, K., Förster, H.-J., Heinrich, W., and Davidson, P. (2006b) The transition from peraluminous to peralkaline granitic melts: Evidence from melt inclusions and accessory minerals. *Lithos*, 91, 137–149.
- Thomas, R., Davidson, P., and Schmidt, C. (2011) Extreme alkali bicarbonate- and carbonate-rich fluid inclusions in granite pegmatite from the Precambrian Ronne granite, Bornholm Island, Denmark. *Contributions to Mineralogy and Petrology*, 161, 315–329.
- Woodward, L.A., and Roberts, H.L. (1956) The Raman and infra-red absorption spectra of osmium tetroxide. Relation to the structure of the perchlorate and tungstate ions in aqueous solution. *Transactions of the Faraday Society*, 52, 615–619.
- Xiong, X., Li, J.K., Wang, D.H., Li, S.P., and Lin, H. (2019) Fluid characteristics and evolution of the Zhawulong granitic pegmatite lithium deposit in the Ganzi-Songpan region, Southwestern China. *Acta Geologica Sinica, English Edition*, 93, 943–954.

MANUSCRIPT RECEIVED NOVEMBER 24, 2020

MANUSCRIPT ACCEPTED JANUARY 31, 2021

MANUSCRIPT HANDLED BY DANIEL R. NEUVILLE